typeset using JPSJ.sty <ver.1.0b>

A Fully Relativistic Full-Potential LCAO Method for Solids

Shugo Suzuki and Kenji Nakao

Institute of Materials Science, University of Tsukuba, Tsukuba 305-8573

(Received January 12, 1999)

We present a fully relativistic full-potential linear-combination-of-atomic-orbitals method for solids based on the density-functional theory within the local-density approximation. We solve the Dirac-Kohn-Sham equations directly, handling not only the indirect relativistic effect but also the effect due to the spin-orbit coupling self-consistently. We apply the present method to Au and InSb and compare the results with those of experimental and other theoretical studies. Consequently, we show that the agreement is good and the present method is capable of obtaining reliable results in studying the structural and electronic properties of solids.

KEYWORDS: fully relativistic calculations, full-potential calculations, LCAO method, density-functional theory, band calculations, structure optimizations

§1. Introduction

Relativistic effects have strong impacts on the structural and electronic properties of the materials with heavy elements. One important effect is the indirect relativistic effect; the strong contraction of core-electron orbitals due to relativity results in the expansion of valence-electron orbitals, especially of d and f orbitals.[1)] This largely affects the interatomic distances, the cohesive energies, the one-electron energies, etc.[2)] This effect can be handled within the scalar relativistic calculations.[3)] Another important effect is due to the spin-orbit coupling, which plays essential roles in magnetocrystalline anisotropy,[4)] magnetic circular dichroism,[5)] magneto-optic Kerr effect,[6)] etc. In contrast with the indirect relativistic effect, the spin-orbit coupling requires more elaborate treatment beyond the scalar relativistic calculations, i.e., the fully relativistic calculations.

To date, several fully relativistic methods have been developed in various schemes for the first-principles all-electron calculations for solids: the augmented-plane-wave (APW) method,[7–11)] the linearized muffin-tin-orbital (LMTO) method,[12–16)] the Korringa-Kohn-Rostoker (KKR) method,[17–24)] and the linear-combination-of-atomic-orbitals (LCAO) method.[25–28)] In these methods, the term "fully relativistic" is used in several ways. One method solves the Dirac-Kohn-Sham equations directly.[24)] Another method employs the scalar relativistic calculations for the self-consistent calculations and then applies the second-variation method to handle the spin-orbit coupling.[11)] Furthermore, some other methods use the transformations of the Dirac operator,[26–28)]

e.g., the Foldy-Wouthuysen-Tani transformation. In the present study, we use the term "fully relativistic" in the first sense as in ref. 24.

In the LCAO scheme, a serious disease, however, exists in performing relativistic calculations. This disease is known as the variational collapse[29] and is caused by the spurious mixing of negative-energy states.

Several approaches are available to avoid this disease.[29] One approach is to use the squared Dirac operator.[25] Another approach is to transform the Dirac operator into other forms.[26–28] A third approach is to choose basis functions appropriately so that they have positive energies. In particular, this choice can be achieved automatically if we use the numerical-type orbitals (NTOs) constructed by solving the Dirac-Kohn-Sham equations for atoms. This approach has been used successfully in the fully relativistic LCAO method for molecules.[30] No attempts have, however, been made so far to develop a fully relativistic LCAO method for solids with the third approach.

A remarkable advantage of the use of the NTOs in the third approach in a fully relativistic LCAO method is that the basis functions have positive energies and thus have desirable features to avoid the variational collapse as already mentioned in the above. Furthermore, the basis functions transform smoothly to those in the nonrelativistic limit if we increase the speed of light gradually in a hypothetical way. This is also an important feature to avoid the variational collapse.[29]

In spite of these advantages of the NTOs, the LCAO methods with this type of basis functions had been suffered from the difficulty in performing full-potential calculations not only for solids but also for molecules until several useful techniques were developed.[31–38] One important technique is the atomic partitioning method,[32–35,37,38] which enables us to calculate the three-dimensional numerical integration efficiently. Another important technique is the method of solving the Poisson equation accurately,[36,38] which is indispensable for performing full-potential calculations. The development of these techniques has opened the way to study the structural and electronic properties of molecules with the NTOs. Recently, we have extended these techniques to the density-functional calculations of solids within the nonrelativistic formulation and have shown they are also useful for studying the structural and electronic properties of solids.[39]

The purpose of the present study is to present a fully relativistic full-potential LCAO method for solids by extending our previous nonrelativistic full-potential LCAO method for solids. We show that the present method is useful for studying the structural and electronic properties of solids with heavy elements by applying the method to Au and InSb. In §2, we describe the method. We next give the results of the application to Au and InSb in §3. Finally, we give conclusions in §4.

§2. Method

The fully relativistic density-functional calculations of a solid are performed by solving the Dirac-Kohn-Sham equations in a self-consistent way:[40–44)]

$$\left[c\boldsymbol{\alpha}\cdot\boldsymbol{p}+(\beta-I)mc^2+V_{\rm es}(\boldsymbol{r})+V_{\rm xc}(\boldsymbol{r})+\beta\boldsymbol{\Sigma}\cdot\boldsymbol{B}_{\rm xc}(\boldsymbol{r})\right]\psi_n^{\boldsymbol{k}}(\boldsymbol{r})=\varepsilon_n^{\boldsymbol{k}}\psi_n^{\boldsymbol{k}}(\boldsymbol{r})\ , \tag{1}$$

$$\rho_{\rm e}(\boldsymbol{r})=\frac{1}{N}\sum_{n\boldsymbol{k}}f_n^{\boldsymbol{k}}\psi_n^{\boldsymbol{k}}(\boldsymbol{r})^*\psi_n^{\boldsymbol{k}}(\boldsymbol{r})\ , \tag{2}$$

and

$$\boldsymbol{m}_{\rm e}(\boldsymbol{r})=\frac{1}{N}\sum_{n\boldsymbol{k}}f_n^{\boldsymbol{k}}\psi_n^{\boldsymbol{k}}(\boldsymbol{r})^*\beta\boldsymbol{\Sigma}\psi_n^{\boldsymbol{k}}(\boldsymbol{r})\ . \tag{3}$$

In the Dirac operator in the left-hand side of eq. (1), c and m denote the speed of light and the rest mass of an electron, respectively, and the rest energy of an electron, mc^2, is subtracted. Also, $\boldsymbol{\alpha}$ and β are the Dirac matrices in the usual representation.[45)] In the Dirac-Kohn-Sham equations, the one-electron wave function, $\psi_n^{\boldsymbol{k}}(\boldsymbol{r})$, is a four-component spinor and has two quantum numbers, the band index n and the wave vector $\boldsymbol{k}$. The sum of $\boldsymbol{k}$ is performed over the Brillouin zone; the total number of $\boldsymbol{k}$, represented by N, is equal to the total number of the unit cells in the whole solid, provided that the periodic boundary condition is used. In eq. (1), $V_{\rm es}(\boldsymbol{r})$ is the electrostatic potential due to the nucleus charge density, $\rho_{\rm n}(\boldsymbol{r})$, and the electron charge density, $\rho_{\rm e}(\boldsymbol{r})$. Also, $V_{\rm xc}(\boldsymbol{r})$ is the spin-averaged exchange-correlation potential and $\boldsymbol{B}_{\rm xc}(\boldsymbol{r})$ is the exchange-correlation magnetic field due to the spin magnetization density, $\boldsymbol{m}_{\rm e}(\boldsymbol{r})$, which is calculated by using $\boldsymbol{\Sigma}=I_2\otimes\boldsymbol{\sigma}$ where I_2 is the 2×2 unit matrix and $\boldsymbol{\sigma}$ are the usual 2×2 Pauli spin matrices. In the present study, we have used $V_{\rm xc}(\boldsymbol{r})$ and $\boldsymbol{B}_{\rm xc}(\boldsymbol{r})$ given by von Barth and Hedin.[46)] The electron charge density $\rho_{\rm e}(\boldsymbol{r})$ and the spin magnetization density $\boldsymbol{m}_{\rm e}(\boldsymbol{r})$[15,42,47–50)] are given with $\psi_n^{\boldsymbol{k}}(\boldsymbol{r})$ and the occupation number of the level $n\boldsymbol{k}$, $f_n^{\boldsymbol{k}}$, provided that $\psi_n^{\boldsymbol{k}}(\boldsymbol{r})$ is normalized in the unit cell. Given $V_{\rm es}(\boldsymbol{r})$, $V_{\rm xc}(\boldsymbol{r})$, and $\boldsymbol{B}_{\rm xc}(\boldsymbol{r})$, we solve eq. (1) by expanding $\psi_n^{\boldsymbol{k}}(\boldsymbol{r})$ by basis functions as follows.

$$\begin{aligned}\psi_n^{\boldsymbol{k}}(\boldsymbol{r})&=\sum_p\chi_p^{\boldsymbol{k}}(\boldsymbol{r})C_{pn}^{\boldsymbol{k}}\ ,\\ \chi_p^{\boldsymbol{k}}(\boldsymbol{r})&=\sum_u\exp(\mathrm{i}\boldsymbol{k}\cdot\boldsymbol{R}_u)\chi_p(\boldsymbol{r}-\boldsymbol{d}_p-\boldsymbol{R}_u)\ .\end{aligned} \tag{4}$$

Here, $\chi_p(\boldsymbol{r})$ is the p-th atomic orbital which is a four-component spinor obtained numerically as a solution of the Dirac-Kohn-Sham equations for atoms. Also, $\boldsymbol{d}_p+\boldsymbol{R}_u$ represents its position vector in the u-th unit cell. An important merit of the use of this type of atomic orbitals, the NTOs, as the basis functions in the fully relativistic LCAO methods is that we can avoid the variational collapse because the NTOs have positive energies preventing the spurious mixing of negative-energy states into $\psi_n^{\boldsymbol{k}}(\boldsymbol{r})$. Furthermore, another important merit is that we can perfectly describe the

dissociated limit of the constituent atoms within the local-density approximation (LDA), allowing us to calculate cohesive energies accurately. The expansion (4) results in the following generalized eigenvalue problem:

$$\sum_q H_{pq}^{\boldsymbol{k}} C_{qn}^{\boldsymbol{k}} = \varepsilon_n^{\boldsymbol{k}} \sum_q S_{pq}^{\boldsymbol{k}} C_{qn}^{\boldsymbol{k}} \ . \tag{5}$$

The Hamiltonian and the overlap matrices are given by

$$H_{pq}^{\boldsymbol{k}} = \int \chi_p^{\boldsymbol{k}}(\boldsymbol{r})^* \left[c\boldsymbol{\alpha} \cdot \boldsymbol{p} + (\beta - I)mc^2 + V_{\rm es}(\boldsymbol{r}) + V_{\rm xc}(\boldsymbol{r}) + \beta \boldsymbol{\Sigma} \cdot \boldsymbol{B}_{\rm xc}(\boldsymbol{r}) \right] \chi_q^{\boldsymbol{k}}(\boldsymbol{r}) {\rm d}\boldsymbol{r} \tag{6}$$

and

$$S_{pq}^{\boldsymbol{k}} = \int \chi_p^{\boldsymbol{k}}(\boldsymbol{r})^* \chi_q^{\boldsymbol{k}}(\boldsymbol{r}) {\rm d}\boldsymbol{r} \ , \tag{7}$$

respectively. Here, the integrals are performed over the unit cell. The three-dimensional numerical integration in eqs. (6) and (7) is carried out by using the atomic partitioning method.[35,38]

By using the solution of eq. (5), we obtain $\rho_{\rm e}(\boldsymbol{r})$ and $\boldsymbol{m}_{\rm e}(\boldsymbol{r})$ by eqs. (2) and (3), respectively. Then, $V_{\rm es}(\boldsymbol{r})$, $V_{\rm xc}(\boldsymbol{r})$, and $\boldsymbol{B}_{\rm xc}(\boldsymbol{r})$ are constructed from $\rho_{\rm n}(\boldsymbol{r})$, $\rho_{\rm e}(\boldsymbol{r})$, and $\boldsymbol{m}_{\rm e}(\boldsymbol{r})$. Subsequently, $V_{\rm es}(\boldsymbol{r})$, $V_{\rm xc}(\boldsymbol{r})$, and $\boldsymbol{B}_{\rm xc}(\boldsymbol{r})$ are used in the next iteration of the self-consistent calculations. Furthermore, we calculate the total energy as described in the previous paper[39] and also calculate the bulk modulus by fitting the total energies obtained at several lattice constants with the same equation used in ref. 24.[51] Finally, it is worth mentioning that we have developed our code so that we can calculate both the relativistic and nonrelativistic cases by using the same code. This allows us to study the relativistic effects on the structural and electronic properties of solids on the same footing.

§3. Application to Au and InSb

We now apply the present method to the study of the structural and electronic properties of Au and InSb and compare the results of the present study with those of experimental and other theoretical studies. We used 2064 and 3096 points per atom to perform the three-dimensional numerical integration in the real space for Au and InSb, respectively. Also, we used 185 $\mathbf{k}$ points generated with the good-lattice-point method[52] in the full Brillouin zone for Au while 16 $\mathbf{k}$ points generated with the special-point method[53] also in the full Brillouin zone for InSb. Furthermore, we performed the multipolar expansion of the electrostatic potential up to 8.[39]

We chose the basis functions so that they have enough variational flexibility. That is, we used not only the atomic orbitals of neutral atoms but also those of charged atoms. The atomic orbitals used for Au are $1s$, $2s$, $2p$, $3s$, $3p$, $3d$, $4s$, $4p$, $4d$, $4f$, $5s$, $5p$, $5d$, and $6s$ atomic orbitals of neutral Au atoms and $5d$ and $6s$ atomic orbitals of Au^{2+} atoms and $6p$ atomic orbitals of Au^{+} and Au^{3+} atoms. Also, the atomic orbitals used for InSb are $1s$, $2s$, $2p$, $3s$, $3p$, $3d$, $4s$, $4p$, $4d$, $5s$, and $5p$

atomic orbitals of neutral In and Sb atoms and $5s$, $5p$, and $5d$ atomic orbitals of In^{2+} and Sb^{2+} atoms.

We show the results of the present fully relativistic calculations on the optimized lattice constant and the bulk modulus of Au in Table I. Also, we show the results of experimental and other theoretical studies for comparison. Furthermore, the results of nonrelativistic calculations are shown; one is the results of the present study and the other is the results of ref. 28. We first examine the results of the relativistic calculations. The error in the lattice constant obtained by the present study is 0.4 %. All of the theoretical lattice constants are good; even the largest error is less than 1 %. On the contrary, the theoretical bulk moduli are scattered by about 20 %. The error in the present result is 5 %. The largest error is found to be 18 %. This shows that the bulk modulus is a difficult quantity to be calculated accurately. In general, however, it is found that not only the fully relativistic calculations but also the scalar relativistic calculations give good results. This indicates that the spin-orbit coupling plays a minor role in the structural properties of Au. We next compare the results of the relativistic calculations with those of the nonrelativistic calculations. We find that the lattice constant is overestimated by 5 % and the bulk modulus is underestimated by 35 %. This strongly shows the importance of the inclusion of the relativistic effects into the study of the structural properties of Au.

We show the results of the fully relativistic band calculations in Fig. 1 and the results of the nonrelativistic band calculations in Fig. 2; both results are obtained at the experimental lattice constant. We can see that there are two types of band; one is with large dispersion and with s character, namely the s band, and the other is with small dispersion and with d character, namely the d band. Comparing Fig. 1 and Fig. 2, we find that the relativistic effects make the s-band deep and the d band shallow. This is known as the indirect relativistic effect and affects the bond strength between Au atoms strongly as already shown in Table I. Furthermore, we note that the degeneracy occurring at some symmetrical points in the nonrelativistic results is partly lifted in the relativistic results. This is due to the spin-orbit coupling. We next show the d-band width obtained by the present fully relativistic calculations and those obtained by other theoretical studies in Table II. We also show the results of the nonrelativistic calculations. The d-band width is defined as the difference between the first and the fifth energy band at the X point as shown in Figs. 1 and 2. It is found that the three relativistic results with the spin-orbit coupling agree well with each other while the two scalar relativistic results without the spin-orbit coupling differ from the former results noticeably. This shows the importance of the inclusion of the spin-orbit coupling in studying the electronic structures, at least within perturbative treatments. Of course, the results of the nonrelativistic calculations are poor, again showing the importance of the inclusion of the relativistic effects.

Next, we show the results of the present fully relativistic calculations on the optimized lattice

constant and the bulk modulus of InSb in Table III. Also, We show the results of experimental and other theoretical studies for comparison. Furthermore, the results of the present nonrelativistic calculations are shown. We first examine the results of the relativistic calculations. The error in the lattice constant obtained by the present study is 0.2 %. Also, the largest error in the theoretical lattice constants is 2 %. It should, however, be noted that the all-electron calculations give better results than the pseudopotential plane-wave calculations. This has been attributed to the neglect of the partial core correction in the pseudopotential calculations.[62] In general, the agreement of the theoretical lattice constants with the experimental one is good. Also, the agreement of the theoretical bulk moduli with the experimental one is good; the error in the bulk modulus obtained by the present study is 0.6 % and the largest error in the theoretical bulk moduli is 7 %. We next compare the results of the relativistic calculations with those of the nonrelativistic calculations. In contrast with the case of Au, the results of nonrelativistic calculations are not so poor; the error in the lattice constant is 1 % and the error in the bulk modulus is 10 %. This should be due to the fact that In and Sb are not so heavy that the relativistic effects do not play an important role in studying the structural properties of InSb.

We show the results of the fully relativistic band calculations in Fig. 3 and the results of the nonrelativistic band calculations in Fig. 4; both results are obtained at the experimental lattice constant. We should first note that there is no gap in the result of the fully relativistic calculations in agreement with the result Fig. 7(b) in ref. 24. Since actual InSb has a gap, this should be attributed to the error due to LDA which underestimates band gaps. The gap obtained by the nonrelativistic calculations should, therefore, be regarded as an accidental one due to the cancellation between the underestimation by LDA and the overestimation by the neglect of the relativistic effects. In Fig. 3, we can see the effects of the spin-orbit coupling. An obvious one is found as a split of the p-derived valence bands just below the Fermi level and also a split of the semicore bands derived from the $4d$ states of In located at the bottom of the figure. Furthermore, we can also see another effect by the spin-orbit coupling along the X-W-L and Γ-Σ-K, U-X lines; there are slight splits of several bands due to the spin-orbit coupling because InSb has no inversion symmetry so that the bands split at general $\boldsymbol{k}$ points without any symmetry. We next show the one-electron energies at the Γ, X, and L points at the experimental lattice constant obtained by the present study and those obtained by other theoretical studies in Table IV. The agreement of the present fully relativistic results with the fully relativistic full-potential KKR results[24] is good. We also show the results of the scalar relativistic calculations. As seen in the table, this type of treatment can give good results if the spin-orbit coupling is taken into account. It should, however, be noted that the agreement is not good if the spin-orbit coupling is neglected.[62] Furthermore, we can again see the importance of the inclusion of the relativistic effects by comparing with the results of the nonrelativistic calculations also shown in the table.

§4. Conclusions

We developed a fully relativistic full-potential LCAO method for solids based on the density-functional theory within the local-density approximation. We solved the Dirac-Kohn-Sham equations directly, handling not only the indirect relativistic effect but also the effect due to the spin-orbit coupling self-consistently. Applying the present method to Au and InSb, we showed that the method is useful for studying the structural and electronic properties of solids with heavy elements. For Au, we found that not only the fully relativistic calculations but also the scalar relativistic calculations give good results on the structural properties while the nonrelativistic calculations give poor ones. It was, however, found that it is necessary to include the spin-orbit coupling in studying the band structure. For InSb, we found that the relativistic effects do not play an important role in the structural properties while they play an important role in the band structure.

Acknowledgements

One of the authors (S.S.) is grateful to A. J. Freeman, T. Oguchi, R. Asahi, S. J. Youn, and M. Ryzhkov for helpful discussions and suggestions.

References

1) A. J. Freeman and J. P. Desclaux: J. Magn. Magn. Mater. **12** (1979) 11.
2) T. Ziegler, J. G. Snijders, and E. J. Baerends: J. Chem. Phys. **74** (1981) 1271.
3) D. D. Koelling and B. N. Harmon: J. Phys. C: Solid State Phys. **10** (1977) 3107.
4) For example, see M. Kim, L. Zhong, and A. J. Freeman: Phys. Rev. B **57** (1998) 5271.
5) For example, see T. Oguchi, K. Iwashita, and T. Jo: Physica B **237-238** (1997) 374.
6) For example, see T. Kraft, P. M. Oppeneer, V. N. Antonov, and H. Eschrig: Phys. Rev. B **52** (1995) 3561.
7) T. L. Loucks: Phys. Rev. **139** (1965) A1333.
8) T. L. Loucks: Phys. Rev. **143** (1966) 506.
9) L. F. Mathesis: Phys. Rev. **151** (1966) 450.
10) D. D. Koelling: Phys. Rev. **188** (1969) 1049.
11) A. H. Macdonald, W. E. Pickett, and D. D. Koelling: J. Phys. C: Solid State Phys. **13** (1980) 2675.
12) N. E. Christensen: J. Phys. F **8** (1978) L51.
13) C. Godreche: J. Magn. Magn. Mater. **29** (1982) 262.
14) N. E. Christensen: Int. J. Quantum Chem. **25** (1984) 233.
15) H. Ebert: Phys. Rev. B **38** (1988) 9390.
16) H. Ebert, P. Strange, and B. L. Gyorffy: J. Appl. Phys. **63** (1988) 3052.
17) Y. Onodera and M. Okazaki: J. Phys. Soc. Jpn. **21** (1966) 1273.
18) S. Takada: Prog. Theor. Phys. **36** (1966) 224.
19) R. Feder, F. Rosicky, and B. Ackermann: Z. Phys. B **52** (1983) 31.
20) R. Feder, F. Rosicky, and B. Ackermann: Z. Phys. B **53** (1983) 244.
21) P. Strange, J. B. Staunton, and B. L. Gyorffy: J. Phys. C: Solid State Phys. **17** (1984) 3355.
22) H. Ebert, P. Strange, and B. L. Gyorffy: J. Phys. F **18** (1988) L135.
23) X. Wang, X.-G. Zhang. W. H. Butler, G. M. Stocks, and B. N. Harmon: Phys. Rev. B **46** (1992) 9352.
24) S. Bei der Kellen and A. J. Freeman: Phys. Rev. B **54** (1996) 11187.
25) M. Richter and H. Eschrig: Solid State Commun. **72** (1989) 263.
26) X.-F. Zhong, Y.-N. Xu, and W. Y. Ching: Phys. Rev. B **41** (1990) 10545.
27) N. Mainkar, D. A. Browne, and J. Callaway: Phys. Rev. B **53** (1996) 3692.
28) J. C. Boettger: Phys. Rev. B **57** (1998) 8743.
29) W. Kutzelnigg: Int. J. Quantum Chem. **25** (1984) 107.
30) A. Rosen and D. E. Ellis: J. Chem. Phys. **62** (1975) 3039.
31) T. Ziegler and A. Rauk: Theoret. Chim. Acta **46** (1977) 1.
32) C. Satoko: Chem. Phys. Lett. **83** (1981) 111.
33) C. Satoko: Phys. Rev. B **30** (1984) 1754.
34) P. M. Boerrigter, G. te Velde, and E. J. Baerends: Int. J. Quantum Chem. **33** (1988) 87.
35) A. D. Becke: J. Chem. Phys. **88** (1988) 2547.
36) A. D. Becke and R. M. Dickson: J. Chem. Phys. **89** (1988) 2993.
37) F. W. Averill and G. S. Painter: Phys. Rev. B **39** (1989) 8115.
38) B. Delley: J. Chem. Phys. **92** (1990) 508.
39) S. Suzuki and K. Nakao: J. Phys. Soc. Jpn. **66** (1997) 3881.
40) P. Hohenberg and W. Kohn: Phys. Rev. **136** (1964) B864.
41) W. Kohn and L. J. Sham: Phys. Rev. **140** (1965) A1133.

42) A. H. MacDonald and S. H. Vosko: J. Phys. C: Solid State Phys. **12** (1979) 2977.
43) A. H. Rajagopal: J. Phys. C: Solid State Phys. **11** (1978) L943.
44) M. V. Ramana and A. K. Rajagopal: J. Phys. C: Solid State Phys. **12** (1979) L845.
45) W. Greiner: *Relativistic Quantum Mechanics* (Springer-Verlag, Berlin, 1990).
46) U. von Barth and L. Hedin: J. Phys. C: Solid State Phys. **5** (1972) 1629.
47) W. Gordon: Z. Phys. **50** (1928) 630.
48) H. J. F. Jansen: Phys. Rev. B **38** (1988) 8022.
49) J. Forstreuter, L. Steinbeck, M. Richter, and H. Eschrig: Phys. Rev. B **55** (1997) 9415.
50) H. Yamagami, A. Mavromaras, and J. Kübler: J. Phys. Condens. Matter **9** (1997) 10881.
51) F. Birch: J. Geophys. Res. **83** (1978) 1257.
52) L.-K. Hua and Y. Wang: *Applications of Number Theory to Numerical Analysis* (Springer-Verlag, Berlin, 1981).
53) D. J. Chadi and M. L. Cohen: Phys. Rev. B **8** (1973) 5747.
54) *Numerical Data and Functional Relationships in Science and Technology – Crystal and Solid State Physics*, Vol. 17a of *Landolt-Börnstein*, edited by O. Madelung (Springer, Berlin, 1984).
55) M. Sigalas, D. A. Papaconstantopoulos, and N. C. Bacalis: Phys. Rev. B **45** (1992) 5777.
56) M. Methfessel and J. Kübler: J. Phys. F **12**, (1982) 141.
57) C. Elsässer, N. Takeuchi, K. M. Ho, C. T. Chan, P. Braun, and M. Fahnle: J. Phys. Condens. Matter **2** (1990) 4371.
58) A. Khein, D. J. Singh, and C. J. Umrigar: Phys. Rev. B **51** (1995) 4105.
59) T. Korhonen, M. J. Puska, and R. M. Nieminen: Phys. Rev. B **51** (1995) 9526.
60) M. J. Mehl and D. A. Papaconstantopoulos: Phys. Rev. B **54** (1996) 4519.
61) A. H. MacDonald, J. M. Daams, S. H. Vosko, and D. D. Koelling: Phys. Rev. B **25** (1982) 713.
62) S. Massidda, A. Continenza, A. J. Freeman, T. M. de Pascale, and F. Meloni: Phys. Rev. B **41** (1990) 12079.
63) S. B. Zhang and M. L. Cohen: Phys. Rev. B **35** (1987) 7604.

Figure Captions

Fig. 1. Results of the fully relativistic band calculations of Au at the experimental lattice constant. The dotted line represents the Fermi level.

Fig. 2. Results of the nonrelativistic band calculations of Au at the experimental lattice constant. The dotted line represents the Fermi level.

Fig. 3. Results of the fully relativistic band calculations of InSb at the experimental lattice constant. The dotted line represents the Fermi level.

Fig. 4. Results of the nonrelativistic band calculations of InSb at the experimental lattice constant. The dotted line represents the energy of the top of the valence bands.

Table I. Lattice constant in Å and bulk modulus in GPa of Au.

	Lattice constant	Bulk modulus
Expt.[a)]	4.078	173.2
This work[b)]	4.061	182
Ref. 24[c)]	4.050	190
Ref. 55[d)]	4.069	168.9
Ref. 56[e)]	4.057	
Ref. 57[f)]	4.070	182
Ref. 28[g)]	4.039	196
Ref. 58[h)]	4.053	198
Ref. 59[i)]	4.064	193
Ref. 60[j)]	4.059	205
This work[k)]	4.286	114
Ref. 28[l)]	4.274	112

a) Reference 54.

b) Fully relativistic full-potential LCAO calculations.

c) Fully relativistic full-potential KKR calculations.

d) Scalar relativistic APW calculations.

e) Scalar relativistic augmented-spherical-wave calculations.

f) Pseudopotential mixed-basis calculations.

g) Scalar relativistic full-potential LCAO calculations.

h) Scalar relativistic full-potential linearized APW calculations.

i) Scalar relativistic full-potential LMTO calculations.

j) Scalar relativistic full-potential linearized APW calculations.

k) Nonrelativistic full-potential LCAO calculations.

l) Nonrelativistic full-potential LCAO calculations.

Table II. d-band width in eV of Au.

	d-band width
This work[a)]	6.28
Ref. 24[b)]	6.15
Ref. 61[c)]	6.31
Ref. 55[d)]	5.89
Ref. 28[e)]	5.85
This work[f)]	5.02
Ref. 28[g)]	5.01

a) Fully relativistic full-potential LCAO calculations.

b) Fully relativistic full-potential KKR calculations.

c) Scalar relativistic APW calculations with the spin-orbit coupling.

d) Scalar relativistic APW calculations without the spin-orbit coupling.

e) Scalar relativistic full-potential LCAO calculations without the spin-orbit coupling.

f) Nonrelativistic full-potential LCAO calculations.

g) Nonrelativistic full-potential LCAO calculations.

Table III. Lattice constant in Å and bulk modulus in GPa of InSb.

	Lattice constant	Bulk modulus
Expt.[a)]	6.479	48.3
This work[b)]	6.463	48
Ref. 24[c)]	6.448	45
Ref. 62[d)]	6.464	48
Ref. 62[e)]	6.36	48
Ref. 63[f)]	6.359	47
This work[g)]	6.542	53

a) Reference 54.

b) Fully relativistic full-potential LCAO calculations.

c) Fully relativistic full-potential KKR calculations.

d) Scalar relativistic full-potential linearized APW calculations.

e) Pseudopotential plane-wave calculations.

f) Pseudopotential plane-wave calculations.

g) Nonrelativistic full-potential LCAO calculations.

Table IV. One-electron energies in eV of InSb at Γ, X, and L.

	This work[a)]	Ref. 24[b)]	Ref. 62[c)]	Ref. 62[d)]	This work[e)]
Γ_{15c}	2.82	2.83			2.89
	2.38	2.39			
Γ_{1c}	−0.65	−0.66	−0.74	−0.47	1.00
Γ_{15v}	0.00	0.00	0.00	0.00	0.00
	−0.78	−0.77	−0.76		
Γ_{1v}	−11.06	−11.05	−11.11	−10.83	−10.08
Γ_{12v}	−14.42	−14.26		−14.64	−15.49
Γ_{25v}	−14.48	−14.34		−14.73	−15.57
	−15.29	−15.15			
X_{3c}	0.99	0.94			1.41
X_{1c}	0.98	0.91	1.04	1.28	1.31
X_{5v}	−2.46	−2.49	−2.48	−2.28	−2.28
	−2.64	−2.67	−2.65		
X_{3v}	−6.29	−6.24	−6.29	−6.01	−5.58
X_{1v}	−9.08	−9.05	−9.15	−8.88	−7.96
L_{3c}	3.62	3.51			3.69
	3.42	3.33			
L_{1c}	0.15	0.15	0.13	0.39	1.08
L_{3v}	−1.04	−1.05	−1.06	−1.04	−1.01
	−1.53	−1.53	−1.54		
L_{1v}	−5.98	−5.93	−5.98	−5.70	−5.39
L_{1v}	−9.69	−9.68	−9.75	−9.48	−8.63

a) Fully relativistic full-potential LCAO calculations.

b) Fully relativistic full-potential KKR calculations.

c) Scalar relativistic full-potential linearized APW calculations with the spin-orbit coupling.

d) Scalar relativistic full-potential linearized APW calculations without the spin-orbit coupling.

e) Nonrelativistic full-potential LCAO calculations.

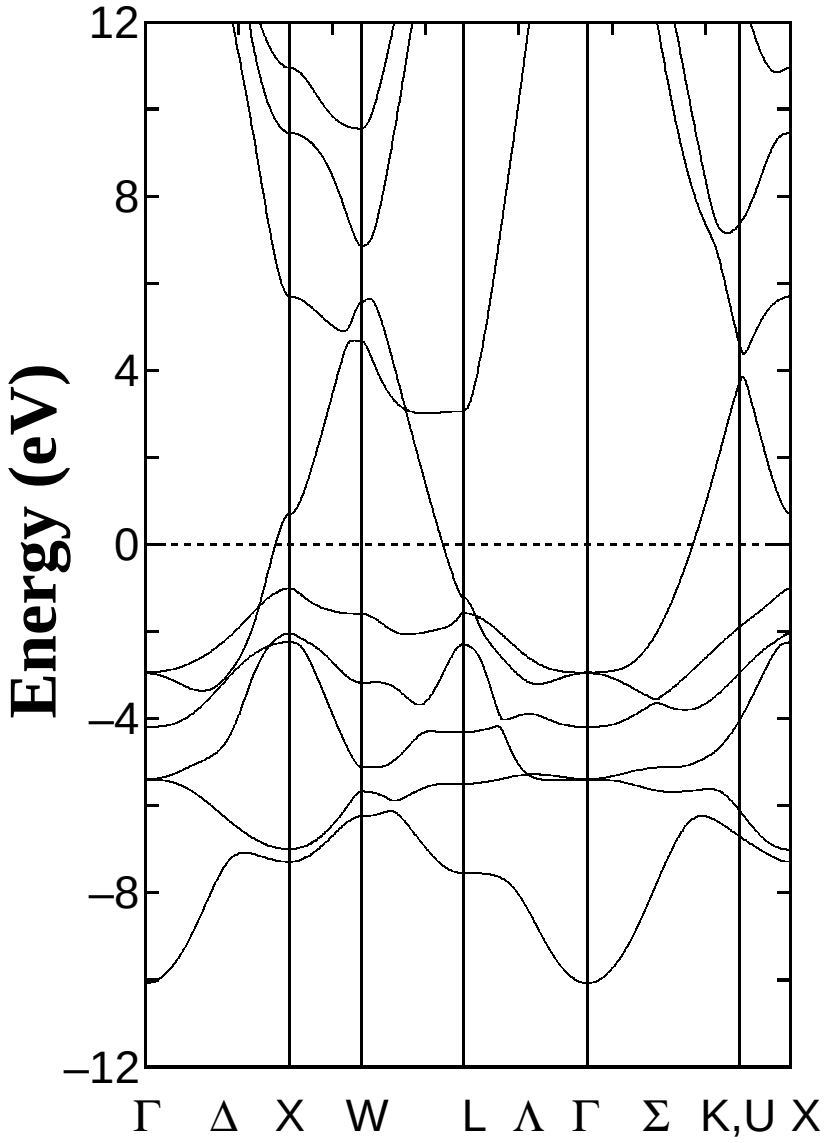

Fig. 1

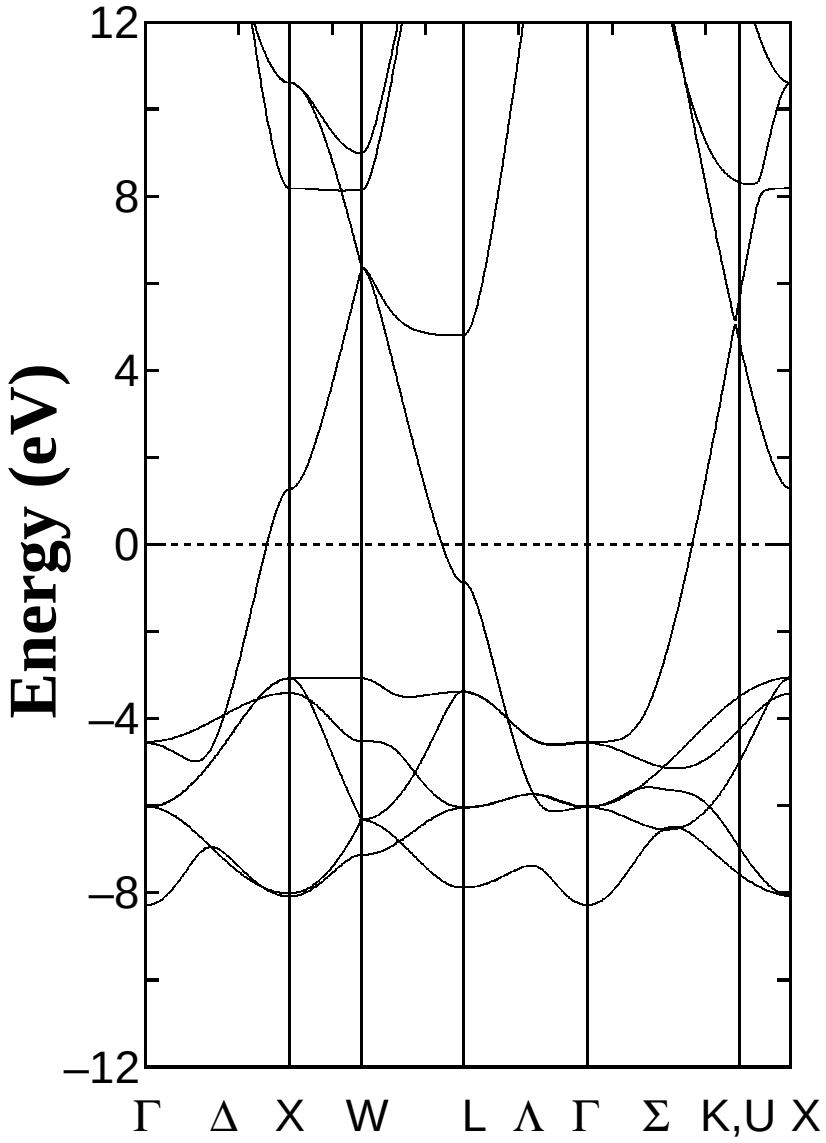

Fig. 2

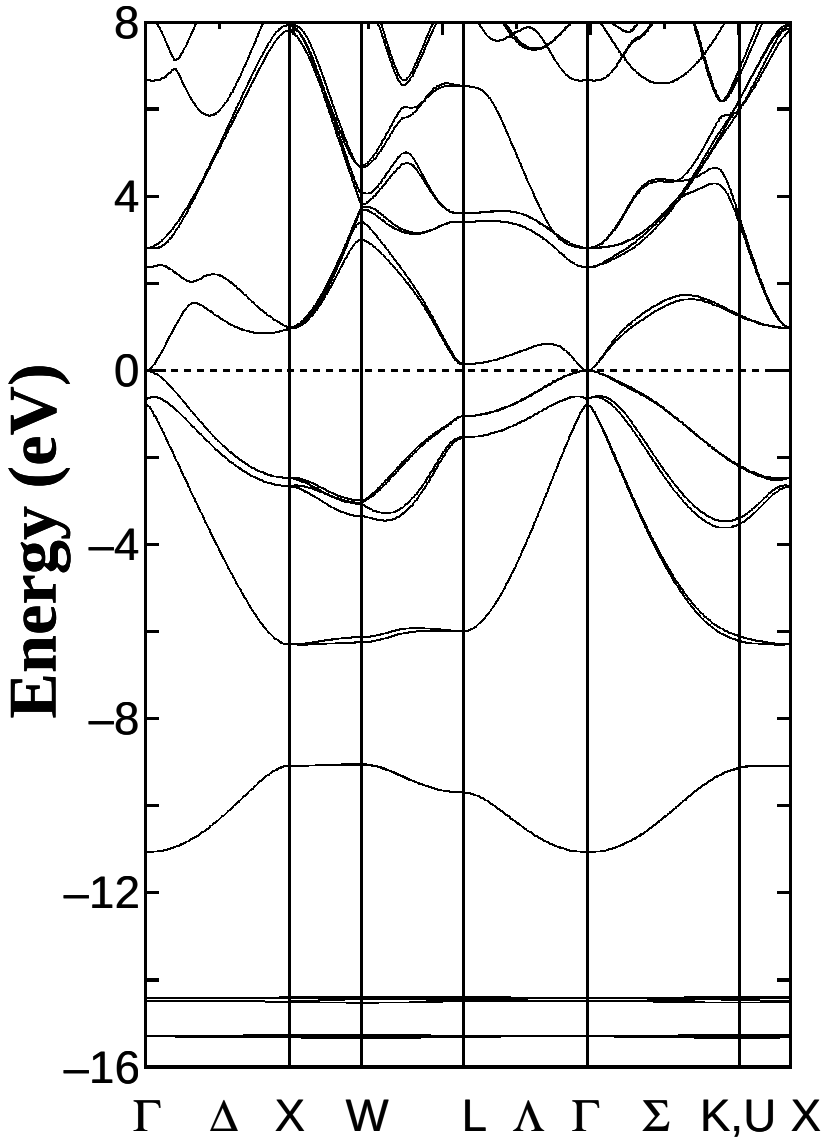

Fig. 3

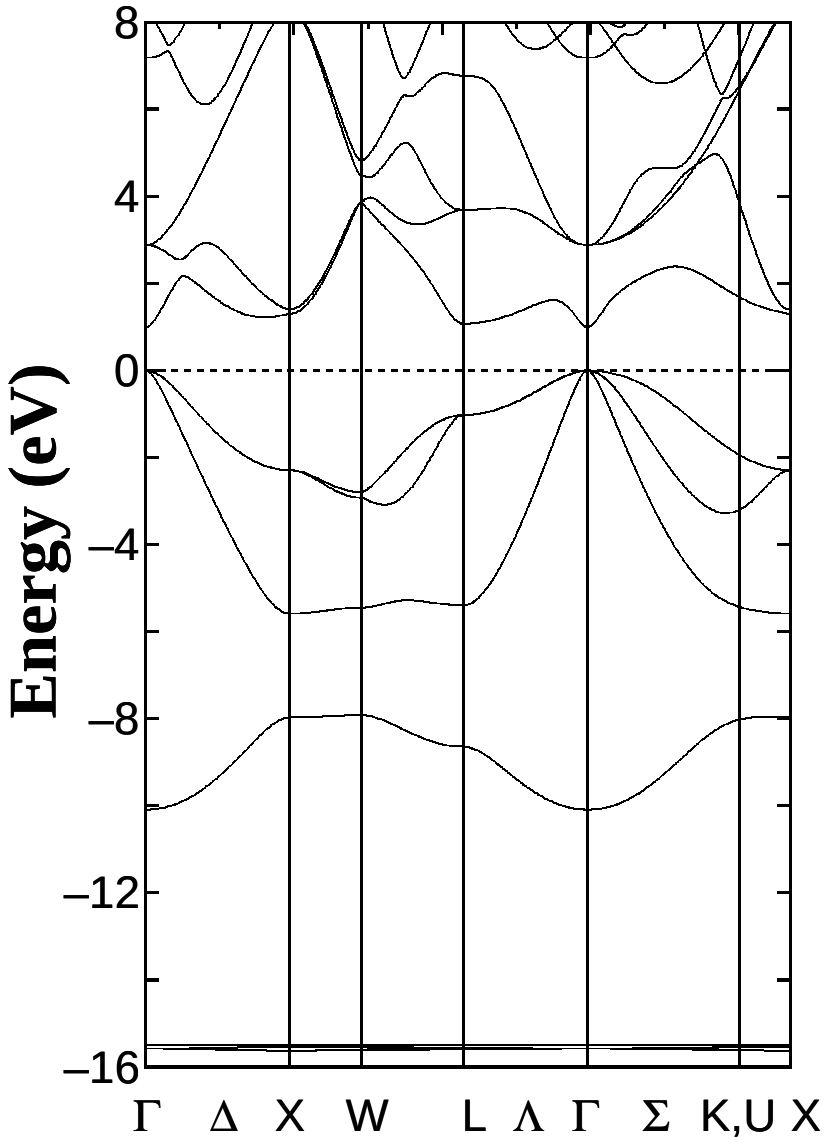

Fig. 4